

Article

# Antimony Oxide-Doped $0.99\text{Pb}(\text{Zr}_{0.53}\text{Ti}_{0.47})\text{O}_3$ – $0.01\text{Bi}(\text{Y}_{1-x}\text{Sb}_x)\text{O}_3$ Piezoelectric Ceramics for Energy-Harvesting Applications

Iqbal Mahmud<sup>1</sup>, Man-Soon Yoon<sup>2</sup> and Soon-Chul Ur<sup>2,\*</sup>

<sup>1</sup> Department of Electrical and Electronic Engineering, Eastern University, Dhaka 1230, Bangladesh; iqbal.et@easternuni.edu.bd

<sup>2</sup> Department of Materials Science and Engineering/RIC-ReSEM, Korea National University of Transportation, 50 Daehagno, Chungju, Chungbuk 380-702, Korea; relaxor02@naver.com

\* Correspondence: scur@ut.ac.kr; Tel.: +82-43-841-5385

Received: 10 August 2017; Accepted: 14 September 2017; Published: 19 September 2017

**Abstract:** The effects of doping antimony oxides ( $\text{Sb}_2\text{O}_3/\text{Sb}_2\text{O}_5$ ) on the ferroelectric/piezoelectric and energy-harvesting properties of  $0.99\text{Pb}(\text{Zr}_{0.53}\text{Ti}_{0.47})\text{O}_3$ – $0.01\text{BiYO}_3$  (PZT–BY) have been studied. The feasibility of doping  $\text{Sb}_2\text{O}_3$  and  $\text{Sb}_2\text{O}_5$  into the PZT–BY ceramics has also been compared by considering factors such as sintering condition, grain size, density, and electrical properties etc. This work discusses a detailed experimental observation using  $\text{Sb}_2\text{O}_3$ , because  $\text{Sb}_2\text{O}_5$  is relatively expensive and does not follow the stoichiometric reaction mechanism when doped in PZT–BY. The  $\text{Sb}_2\text{O}_3$ -doped specimens were well sintered by oxygen-rich sintering and reached a maximum density of 99.1% of the theoretical value. X-ray diffraction (XRD) analysis showed a complete solid solution for all the specimens. Scanning electron microscope (SEM) observation revealed that the addition of  $\text{Sb}_2\text{O}_3$  inhibits grain growth, and exhibits a denser and finer microstructure. The 0.1 moles of  $\text{Sb}_2\text{O}_3$ -doped ceramic shows a sharp decrease in the dielectric constant ( $\epsilon_{33}^T = 690$ ), while the piezoelectric charge constant ( $d_{33}$ ) and electromechanical coupling factor ( $k_p$ ) maintained high values of 350 pC/N and 66.0% respectively. The relatively higher value of  $d_{33}$  and lower  $\epsilon_{33}^T$  of the  $0.99\text{Pb}(\text{Zr}_{0.53}\text{Ti}_{0.47})\text{O}_3$ – $0.01\text{Bi}(\text{Y}_{0.9}\text{Sb}_{0.1})\text{O}_3$  ceramic resulted in an optimum value of piezoelectric voltage constant ( $g_{33} = 57.4 \times 10^{-3}$  Vm/N) and a high figure of merit ( $d_{33} \times g_{33} = 20075 \times 10^{-15}$  m<sup>2</sup>/N). These values are high compared to recently reported works. Therefore,  $\text{Sb}_2\text{O}_3$ -doped PZT–BY ceramic could be a promising candidate material for the future study of power-harvesting devices.

**Keywords:** calcination; piezoelectric ceramics; dielectric properties; energy-harvesting

## 1. Introduction

The use of renewable energy from different technologies to make a contribution to the world's total energy supply has grown fast. Among different energy conversion technologies, piezoelectric energy-harvesting has received considerable attention for powering small electronic components. The piezoelectric effect is a unique property that allows materials to convert mechanical energy to electrical energy or vice versa. Piezoelectric material selection is crucial in the design of piezoelectric energy harvesters. Numerous researchers are working in this area, but most of the solutions being employed have low power (nW) and high frequency [1,2]. Among the various piezoelectric materials, lead zirconate titanate (PZT) based ceramic is one of the most widely used because of its fast electro-mechanical response, relatively low power requirements, high generative force, and inherent durability [3–7]. Extensive research and development of PZT-based ceramics have been conducted to find such piezoelectric materials [1,7–10]. A variety of parameters is used to compare piezoelectric materials for energy-harvesting, such as electromechanical coupling factor, piezoelectric

charge constant, output voltage, power density, energy-conversion efficiency, and cost and frequency of operation. Among them, energy-conversion efficiency is the most important when designing piezoelectric energy harvesters for real applications [11]. Xu et al. proposed a new figure of merit (FOM), which combines the transduction efficiency and the energy-conversion capacity, for comparing piezoelectric materials for energy-harvesting applications [11]. Priya et al. proposed a FOM for a polycrystalline piezoelectric energy-harvesting device, which can be expressed by the following Equations (1) and (2) [12]:

$$u = 1/2 (d.g) (F/A)^2 \quad (1)$$

$$g = d/\epsilon_{33}^T \quad (2)$$

where  $d$  is the piezoelectric charge constant,  $g$  is the piezoelectric voltage constant,  $\epsilon_{33}^T$  is the dielectric permittivity,  $F$  is the applied force, and  $A$  is the area.

According to Equations (1) and (2), a material with a high  $d$  and a lower  $\epsilon_{33}^T$  will generate high FOM. In general, the piezoelectric charge constant and the dielectric constant increase or decrease concurrently upon modification with dopants or processing techniques [7–10]. However, by modifying the fabrication technique and choosing suitable dopants, it is possible to produce high  $d_{33}$  with low  $\epsilon_{33}^T$ . Previous work has reported on such a piezoelectric ceramic composition of  $(1-x)\text{Pb}(\text{Zr}_{0.53}\text{Ti}_{0.47})\text{O}_3-x\text{BiYO}_3$  [PZT–BY] and its fabrication process [13].

In the present study, PZT–BY composition is further tuned using antimony oxide (both  $\text{Sb}_2\text{O}_3$  and  $\text{Sb}_2\text{O}_5$ ) to improve the FOM. The  $\text{Sb}_2\text{O}_3$ - and  $\text{Sb}_2\text{O}_5$ -doped PZT has had a long history whereby  $\text{Sb}_2\text{O}_3/\text{Sb}_2\text{O}_5$  was doped with other oxides for tailoring piezoelectric/dielectric properties [14–22]. Lonker et al. reported a high electrical output in the lanthanum-doped  $\text{Pb}(\text{Ni}_{1/3}\text{Sb}_{2/3})\text{–PbZrTiO}_3$  system which was comparable to the PZT type 5A [16]. Zhou et al. reported a high electrical output in the  $\text{Sb}_2\text{O}_3$ -doped  $\text{Pb}(\text{Zr}_{0.54}\text{Ti}_{0.46})\text{O}_3$  system [14]. They explained that the ionic radius of  $\text{Sb}^{3+}$  is smaller than that of other trivalence “soft” ions; this may be the most important factor for improving the piezoelectric activity. S. Zahi et al. reported a high electromechanical coupling factor and dielectric constant with relatively higher  $T_c$  in the  $x\text{PbZrO}_3\text{–}(90-x)\text{PbTiO}_3\text{–}10\text{Pb}(\text{Ni}_{1/3}, \text{Sb}_{2/3})\text{O}_3$  ternary system [17]. Dutta et al. studied the structural and electrical properties of  $\text{Sb}^{3+}$ -modified  $[\text{Pb}_{0.92}(\text{La}_{1-2}\text{Sb}_z)_{0.08}(\text{Zr}_{0.65}\text{Ti}_{0.35})_{0.98}]\text{O}_3$  (PLZT) ceramics and provided some interesting ferroelectric and sensing properties [20,21]. Furthermore, Zhou et al. studied the effect of doping  $\text{Sb}_2\text{O}_3$  in  $\text{Pb}(\text{Zr}_{0.54}\text{Ti}_{0.46})\text{O}_3$  and obtained an optimum value of piezoelectric activity with  $d_{33} = 570 \times 10^{-12}$  C/N and piezoelectric voltage constant,  $g_{33} = 32 \times 10^{-3}$  Vm/N [14].

In this work, the effects of doping  $\text{Sb}_2\text{O}_3$  and  $\text{Sb}_2\text{O}_5$  on  $0.99\text{Pb}(\text{Zr}_{0.53}\text{Ti}_{0.47})\text{O}_3\text{–}0.01\text{Bi}[\text{Y}_{(1-x)}\text{Sb}_x]\text{O}_3$  (abbreviated as PZT–BYS( $x$ )) from now on, where  $0 \leq x \leq 0.6$ ) ceramics have been compared in terms of sintering condition and piezoelectric/dielectric properties. Based on comparative studies,  $\text{Sb}_2\text{O}_3$  is selected as a dopant into the PZT–BYS( $x$ ) system. Therefore, detailed experimental observations of  $\text{Sb}_2\text{O}_3$  doping into PZT–BYS( $x$ ) regarding piezoelectric/dielectric, ferroelectric and energy-harvesting properties are evaluated and discussed.

## 2. Materials and Methods

At the first stage, a precursor of  $\text{PbZr}_{0.53}\text{Ti}_{0.47}\text{O}_3$  (PZT) and  $\text{Sb}_2\text{O}_3/\text{Sb}_2\text{O}_5$ -doped  $\text{BiY}_{1-x}\text{Sb}_x\text{O}_3$  [BYS( $x$ ), where  $x = 0.0, 0.1, 0.2, 0.3, 0.4, 0.5, 0.6$ ] was prepared by a conventional solid state method. In the final stage, the precursors of PZT and BYS( $x$ ) was mixed stoichiometrically to fabricate  $0.99\text{Pb}(\text{Zr}_{0.53}\text{Ti}_{0.47})\text{O}_3\text{–}0.01\text{Bi}[\text{Y}_{(1-x)}\text{Sb}_x]\text{O}_3$  (abbreviated as PZT–BYS( $x$ )) containing various amounts of  $\text{Sb}_2\text{O}_3/\text{Sb}_2\text{O}_5$  ( $0 \leq x \leq 0.6$ ). The pre-synthesis method was considered for the fabrication of PZT–BYS( $x$ ) to eliminate the effects associated with the direct co-doping. The stoichiometric amount of the analytical reagent (AR) grade  $\text{Bi}_2\text{O}_3$  (99.9%, High Purity Chemicals, Japan),  $\text{Sb}_2\text{O}_3$  (99.9%, High Purity Chemicals, Japan) and  $\text{Y}_2\text{O}_3$  (99.9%, High Purity Chemicals, Japan) were weighed to synthesize  $\text{Bi}(\text{Y}_{1-x}\text{Sb}_x)\text{O}_3$  [BYS( $x$ )] (where,  $x = 0.0, 0.1, 0.2, 0.3, 0.4, 0.5, 0.6$ ). The BYS( $x$ ) was then ball milled in distilled water using a  $\text{ZrO}_2$  media for 24 h. The same specimens of BYS( $x$ ) were also prepared by using  $\text{Sb}_2\text{O}_5$  (99%,

Samchun Pure Chemical, Mokock-dong Pyeongtaek, Korea). According to the thermogravimetric and differential scanning calorimetry (TG/DSC-Mettler Toledo) analysis, both  $\text{Sb}_2\text{O}_3$  and  $\text{Sb}_2\text{O}_5$ -doped  $\text{BYS}(x)$  powders were calcined at  $800\text{ }^\circ\text{C}$  for 2 h in alumina crucibles. A detailed synthesis process of  $\text{Pb}(\text{Zr}_{0.53}\text{Ti}_{0.47})\text{O}_3$  (PZT) and  $\text{BiYO}_3$  (BY) were described in previous work [13]. The pre-synthesized PZT and  $\text{BYS}(x)$  powders were weighed according to reaction stoichiometry to fabricate PZT– $\text{BYS}(x)$ , and ball-milled for 72 h. The dried powders were pressed as a disk of 15 mm diameter and then cold isostatically pressed (CIP) under a pressure of 147.2 MPa. The pressed pellets were sintered at various temperatures between  $1050\text{ }^\circ\text{C}$  and  $1250\text{ }^\circ\text{C}$  in air and an oxygen ( $\text{O}_2$ ) rich atmosphere. An equimolar mixture of  $\text{PbO}$  and  $\text{ZrO}_2$  inside a covered alumina crucible was used to limit  $\text{PbO}$  loss from pellets during sintering. The sintered specimens were then polished to obtain parallel surfaces and suitable dimensions (diameter/thickness  $\geq 15$ ) to estimate the piezoelectric properties.

The specimens were characterized using an X-ray diffractometer (XRD, D/Max-2500H, Rigaku, Tokyo, Japan and D8 advance, Bruker, Karlsruhe, Germany) with  $\text{Cu K}\alpha$  radiation after sintering. The morphologies and the microstructures for all of the powders and sintered samples were investigated using a scanning electron microscope (Hitachi S-2400, Tokyo, Japan). In order to measure the electrical properties, we used silver paste to form electrodes on both sides of the sample, which was then fired at  $560\text{ }^\circ\text{C}$  for 30 min. For investigating the proper poling conditions, we poled each specimen in stirred silicon oil at  $120\text{ }^\circ\text{C}$  by applying a DC electric field of 3–6 kV/mm for 45 min; subsequently, the sample was aged at  $120\text{ }^\circ\text{C}$  for 3 h. The dielectric and the piezoelectric properties of the aged samples were then measured and evaluated. A preliminary study indicated that the spontaneous polarization was fully saturated under a DC electric field of 4 kV/mm. Therefore, the optimum poling voltage was chosen as 4.0 kV/mm. A standard deviation of the electric properties could exist in the measured samples, so five specimens were prepared for each batch and tested. The piezoelectric coefficient was determined using a  $d_{33}$  meter (IACAS, Model ZJ-6B, Bolingbrook, IL, USA), and the electromechanical and the dielectric properties were calculated by using a resonance/anti-resonance measurement method [15] and an impedance/gain phase analyzer (HP-4194A, Palo Alto, CA, USA). The temperature dependences of the dielectric constant and the dissipation factor over the temperature range from  $-25$  to  $500\text{ }^\circ\text{C}$  were measured using an automated system at 1 kHz, in which an HP-4194A and temperature-control box ( $-40\text{ }^\circ\text{C}$  to  $150\text{ }^\circ\text{C}$ : Delta 9023 chamber,  $150\text{--}500\text{ }^\circ\text{C}$ : Lindberg tube furnace) were controlled by using a computer system. The temperature was measured using a Keithley 740 thermometer via a K-type thermocouple mounted on the samples. The polarization-electric field ( $P$ - $E$ ) behavior was determined using a Precision LC system (Radiant Technology, Model: 610E, Walden, NY, USA).

### 3. Results and Discussion

#### 3.1. X-ray Diffraction (XRD) Analysis of Pre-Synthesized PZT and $\text{Bi}[\text{Y}_{(1-x)}\text{Sb}_x]\text{O}_3$

Figure 1a,b shows the X-ray diffraction (XRD) patterns of pre-synthesized  $\text{Sb}_2\text{O}_3$ -doped  $\text{Bi}[\text{Y}_{(1-x)}\text{Sb}_x]\text{O}_3$  [ $\text{BYS}(x)$ ] (where  $x = 0.0, 0.1, 0.2, 0.3, 0.4, 0.5$  and  $0.6$ ) and  $\text{Pb}(\text{Zr}_{0.53}\text{Ti}_{0.47})\text{O}_3$  [PZT], respectively. For clarity, only  $\text{Sb}_2\text{O}_3$ -doped  $\text{BYS}(x)$  is presented here. The reaction mixture of  $\text{BYS}(x)$  was characterized by thermogravimetry and differential scanning calorimetry (TG–DSC) to locate the formation temperature. Based on the TG–DSC analysis, undoped  $\text{BiYO}_3$  (BY) and PZT was calcined at  $850\text{ }^\circ\text{C}$ , whereas both  $\text{Sb}_2\text{O}_3$  and  $\text{Sb}_2\text{O}_5$ -doped BY was calcined at  $800\text{ }^\circ\text{C}$  for 2 h. In Figure 1a it can be seen that the major phase formed for the  $\text{BYS}(x)$  could be related only to the diffraction peak given for  $\text{BiYO}_3$  [JCPDS No. 271047]. However, a tiny peak of  $\text{Y}_3\text{Sb}_5\text{O}_{12}$  [JCPDS No. 0430160],  $\text{Bi}_2\text{O}_3$  [JCPDS No. 0270052],  $\text{Y}_2\text{O}_3$  [JCPDS No. 0431036], and  $\text{BiSbO}_4$  [JCPDS No. 0480469] was observed in the XRD patterns. Moreover, it can be seen that the intensity and the number of second phases increase with increasing  $\text{Sb}_2\text{O}_3$  content. Therefore, the XRD studies indicate that the solubility of  $\text{Sb}_2\text{O}_3$  in BY is limited to a certain range. According to Shannon's effective radius [23],  $\text{Y}^{3+}$  and  $\text{Sb}^{3+}$  with a coordination number of six have radii of 0.90 and 0.76 Å, respectively. The difference in radii

between  $Y^{3+}$  and  $Sb^{3+}$  ions is greater than 15%. Therefore, it is not easy for  $Sb^{3+}$  to enter into  $Y^{3+}$ , and the solubility of  $Sb^{3+}$  in the system would be limited. On the other hand, the calcined PZT powder was fully stabilized to the perovskite structure (JCPDS No. 01-070-4264) without any second phases.

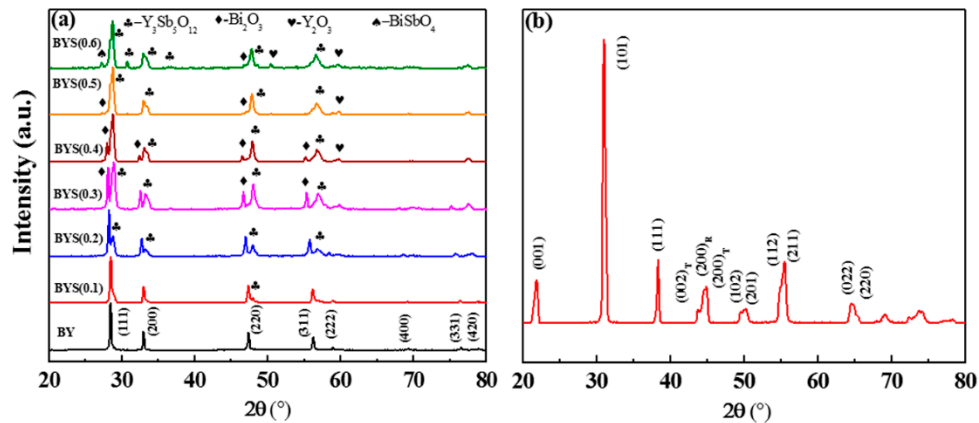


**Figure 1.** X-ray diffraction (XRD) patterns of (a)  $Sb_2O_3$ -doped  $Bi[Y_{1-x}Sb_x]O_3$  and (b)  $Pb(Zr_{0.53}Ti_{0.47})O_3$  calcined at different temperatures.

### 3.2. Comparative Study of $Sb_2O_3$ and $Sb_2O_5$ Doping on the PZT–BY System

$0.99Pb(Zr_{0.53}Ti_{0.47})O_3-0.01Bi[Y_{(1-x)}Sb_x]O_3$  (abbreviated as PZT–BYS( $x$ ) from now on, where  $x = 0.0, 0.1, 0.2, 0.3, 0.4, 0.5,$  and  $0.6$  moles) ceramics were sintered in air and an  $O_2$ -rich atmosphere to investigate the  $Sb_2O_3$  and  $Sb_2O_5$ -doping effects on the microstructure and electrical properties. Figure 2 shows the microstructure for the fracture surfaces of  $Sb_2O_3$  and  $Sb_2O_5$ -doped PZT–BYS(0.1) ceramic sintered at  $1170\text{ }^\circ\text{C}$  in different sintering atmospheres. In addition, the piezoelectric, dielectric, ferroelectric and energy-harvesting parameters of same specimens have been listed in Table 1. From Table 1, it is clear that the piezoelectric properties of  $Sb_2O_5$ -doped specimens sintered in an air atmosphere and  $Sb_2O_3$ -doped specimens sintered in an  $O_2$ -rich atmosphere show higher values than the  $Sb_2O_3$ -doped specimen sintered in air. It may be considered that the presence of oxygen during sintering reduced the porosity and resulted in dense microstructures. Therefore, among other reasons like pre-synthesis, doping, etc., sintering in an oxygen-rich atmosphere is an essential factor for relatively higher piezoelectric properties as well as higher FOM.

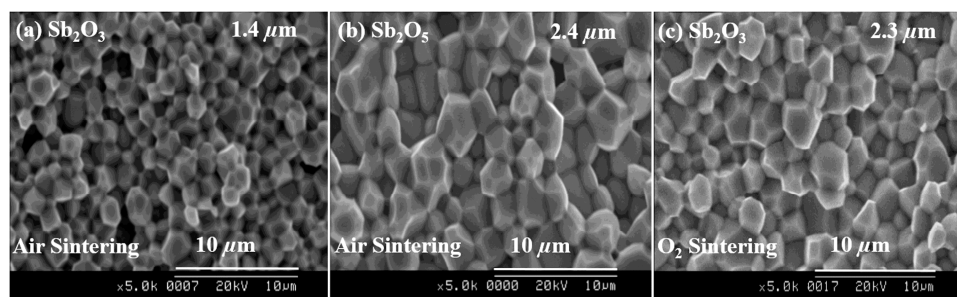


**Figure 2.** SEM (Scanning Electron Microscope) images of the fracture surface of  $Sb_2O_3$  and  $Sb_2O_5$ -doped PZT–BYS(0.1) ceramics sintered in different atmospheres (sintered temperature  $1170\text{ }^\circ\text{C}$ ). PZT–BYS:  $0.99Pb(Zr_{0.53}Ti_{0.47})O_3-0.01Bi[Y_{(1-x)}Sb_x]O_3$ .

**Table 1.** The piezoelectric, dielectric and energy-harvesting parameters of  $\text{Sb}_2\text{O}_3$  and  $\text{Sb}_2\text{O}_5$ -doped PZT-BYS(0.1) ceramics sintered in air and in an  $\text{O}_2$ -rich atmosphere. PZT-BYS:  $0.99\text{Pb}(\text{Zr}_{0.53}\text{Ti}_{0.47})\text{O}_3-0.01\text{Bi}[\text{Y}_{(1-x)}\text{Sb}_x]\text{O}_3$ .

Doping	Sintering Temp. ( $^{\circ}\text{C}$ )	Sintering Condition	Grain Size ( $\mu\text{m}$ )	Density (g/cc)	$d_{33}$ (pC/N)	$\epsilon_{33}^T$	$k_p$ (%)	$g_{33} \times 10^{-3}$ (Vm/N)	$d_{33} \times g_{33}$ ( $10^{-15} \text{ m}^2/\text{N}$ )
$\text{Sb}_2\text{O}_5$	1170	air	2.4	7.94	346	753	65.1	51.9	17,971
$\text{Sb}_2\text{O}_3$		air	1.4	7.88	335	793	63.6	47.7	15,987
$\text{Sb}_2\text{O}_3$		oxygen	2.3	7.96	350	738	64.8	53.3	18,519

In Figure 2, uniform, fine-grained, and almost pore-free microstructures can be seen for  $\text{Sb}_2\text{O}_5$ -doped specimens when sintered in the air atmosphere and for  $\text{Sb}_2\text{O}_3$ -doped samples when sintered in the  $\text{O}_2$ -rich atmosphere. On the other hand,  $\text{Sb}_2\text{O}_3$ -doped specimens sintered in the air have small (approx.  $1.4 \mu\text{m}$ ) and loosely bonded grains. Since the dielectric properties are directly associated with grain size, the air-sintering of the  $\text{Sb}_2\text{O}_3$  sample has a smaller average grain size and shows a higher value of  $\epsilon_{33}^T$ . A similar observation was also explained by Uchino et al. [24]. Subsequently, higher  $\epsilon_{33}^T$  produces a lower FOM according to Equation (1), therefore, doping  $\text{Sb}_2\text{O}_3$  and sintering in the presence of air is not favorable or advantageous in the present case. On the contrary,  $\text{Sb}_2\text{O}_5$  is relatively expensive and does not follow the stoichiometric reaction mechanism when doped in PZT-BY. Therefore, according to the experimental results and discussions above,  $\text{Sb}_2\text{O}_3$  is considered as a substituent for  $\text{Y}^{3+}$  in the PZT-BYS( $x$ ) and also an  $\text{O}_2$ -assisted sintering atmosphere was selected. Hence, a detailed analysis of the crystal structure, microstructure, piezoelectric/dielectric properties, and ferroelectric properties of the  $\text{Sb}_2\text{O}_3$ -doped PZT-BYS( $x$ ) specimens sintered in the  $\text{O}_2$  atmosphere will be discussed in the next sections.

### 3.3. Effects of Pre-Synthesized BYS( $x$ ) Content on the Densities of PZT-BYS( $x$ ) Ceramics

Figure 3 shows the density of PZT-BYS( $x$ ) ceramics sintered at various temperatures as a function of  $\text{Sb}_2\text{O}_3$  content. It is well known that electrical properties are directly related to density. Therefore, a detailed experiment was conducted to find out the optimum sintering temperature at which these ceramics reached their maximum density. From Figure 3, it is clear that the ceramics are well sintered to high densities between 1150 and 1170  $^{\circ}\text{C}$ . At  $x = 0.1-0.3$ , PZT-BYS( $x$ ) ceramics showed the highest density at about 1150  $^{\circ}\text{C}$ . At  $x = 0.4-0.6$ , the density reached its maximum at 1170  $^{\circ}\text{C}$ . As the piezoelectric and dielectric properties are closely related to the microstructure, and sintered density, a detailed investigation of crystal structure, microstructure, piezoelectric/dielectric and ferroelectric properties of PZT-BYS( $x$ ) ceramics sintered at their optimum temperature will be considered and discussed in the next sections.

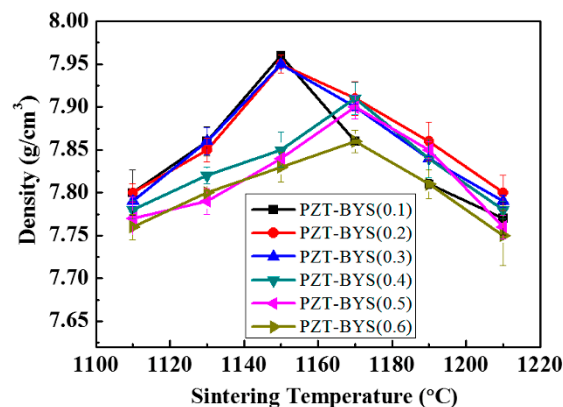


**Figure 3.** Density of PZT-BYS( $x$ ) ceramics sintered in an  $\text{O}_2$ -rich atmosphere at different temperatures.

### 3.4. Effects of Pre-Synthesized BY $S(x)$ on the Crystal Structure and Microstructure of PZT–BY $S(x)$ Ceramics

The XRD patterns of PZT–BY $S(x)$  ceramics sintered at their optimum temperatures are shown in Figure 4a. In these patterns, no detectable traces of the pyrochlore or other impurities were observed. Additionally, asymmetry and/or peak splitting in 111 and 200 reflections indicate all of the compositions are exhibiting rhombohedral–tetragonal phase coexistence [14,15,17]. Quantitative analysis of possible change in relative phase fraction as a function of BY $S$  is not within the scope of this work. Nevertheless, the enlarged XRD patterns in Figure 4b indicated that the decrease in 002 reflection with an increasing amount of  $Sb_2O_3$  is possibly related to the decrease in volume fraction of the long c-axis of the tetragonal unit cell.

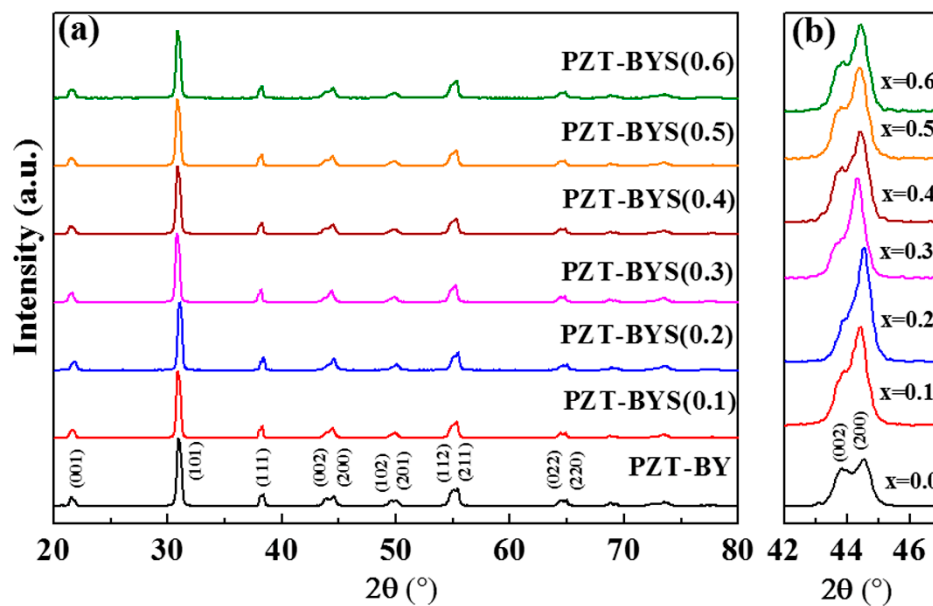


**Figure 4.** (a) X-ray diffraction patterns of  $Sb_2O_3$ -doped PZT–BY $S(x)$  ( $0.1 \leq x \leq 0.6$ ) ceramics sintered at optimum temperature for 2 h, and (b) enlarged portion of XRD at a selected  $2\theta$  angle.

Figure 5 shows the microstructures of the fracture surface containing various amounts of  $Sb_2O_3$  content sintered at an optimum temperature at which maximum density was obtained. A significant change in grain size was observed with the addition of  $Sb_2O_3$ . The microstructures of the sintered samples are uniform, dense and consistent with the measured density. In the previous work, it was reported that the addition of a small amount of BY abruptly decreases the grain size of PZT due to the pinning effect of the second phase [13]. In the present case, the addition of  $Sb_2O_3$  doping on PZT–BY $S(x)$  shows a further decrease in grain size. The average grain size of specimens is decreased with the increasing amount of  $Sb_2O_3$ . From Figure 5b, it can be seen that the microstructure of the specimen doped with 0.1 moles of  $Sb_2O_3$  shows higher uniformity with fine grain size, and an average grain size of 2.2  $\mu m$  was observed. On further addition of  $Sb_2O_3$  content, as shown in Figure 5c–g, the average grain size abruptly decreased to approximately  $\sim 1.7 \mu m$  at  $x = 0.2$ – $0.3$  moles and approximately 1.4  $\mu m$  for  $x = 0.4$ – $0.6$  moles. This reduction of grain size can be interpreted as a pinning effect of the secondary phases ( $Y_3Sb_5O_{12}$ ,  $Bi_2O_3$ ,  $Y_2O_3$ , and  $BiSbO_4$ ) as indicated in XRD patterns in Figure 1a.

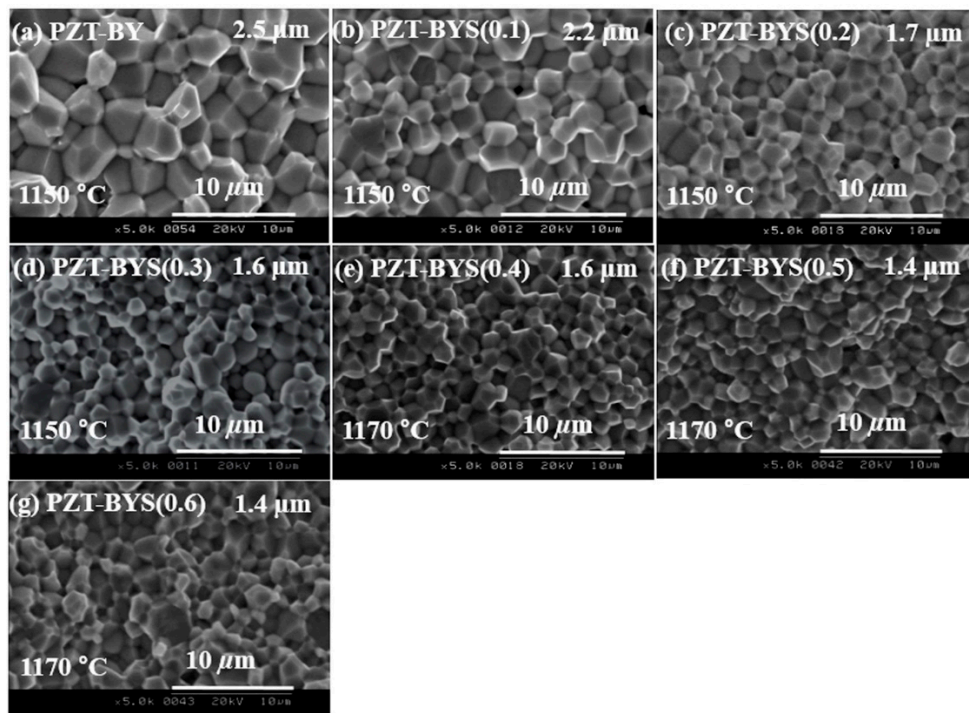


**Figure 5.** SEM images of fracture surface of  $\text{Sb}_2\text{O}_3$ -doped PZT-BYS ( $0.0 \leq x \leq 0.6$ ) specimens sintered at optimum temperature.

The optimized density of sintered PZT-BYS( $x$ ) ceramics is listed in Table 2. The relative densities of the  $\text{Sb}_2\text{O}_3$ -doped specimens were higher than 98% of the theoretical density, indicating the development of dense microstructure in all of these compositions. However, it can be observed that the compositions with  $x = 0.1$  show relatively higher density than other compositions. This may be attributed to the relatively uniform grain size with scarcer porosity at  $x = 0.1$ , which promotes densification. Further addition of  $\text{Sb}_2\text{O}_3$  into the compositions decreases the density again. The SEM investigations, as in Figure 5, revealed supporting evidence that the ceramics with higher  $\text{Sb}_2\text{O}_3$  ( $x > 0.1$  moles) compositions contain small and loosely bonded grains. Evidently, this could be a reason for the much lower density of these compositions. Among all the compositions, a peak density of  $7.96 \text{ g/cm}^3$  (99.1% of the theoretical density) was obtained at  $x = 0.1$ .

**Table 2.** The ferroelectric, dielectric and piezoelectric properties of the PZT-BYS( $x$ ) ceramics at the optimum sintering temperature.

Composition	Sintering Temp. (°C)	Grain Size (μm)	$\rho$ (g/cc)	$d_{33}$ (pC/N)	$\epsilon_{33}^T$	$k_p$ (%)	$P_r$ ( $\mu\text{C/cm}^2$ )	$E_c$ (kV/cm)	$T_c$ (°C)	$\tan\delta$ (1 kHz) 25 °C [ $10^{-3}$ ]
PZT-BYS(0.0)	1150	2.5	7.91	324	742	63.5	45.6	11.5	373	0.0197
PZT-BYS(0.1)	1150	2.2	7.96	350	689	66	45.8	12.0	369	0.0213
PZT-BYS(0.2)	1150	1.7	7.95	352	774	65.5	46.3	12.9	365	0.0226
PZT-BYS(0.3)	1150	1.6	7.95	355	804	65.2	46.9	13.6	361	0.0201
PZT-BYS(0.4)	1170	1.6	7.91	360	835	64.9	47	13.8	361	0.0286
PZT-BYS(0.5)	1170	1.4	7.9	366	867	64.7	47.2	14.0	357	0.0215
PZT-BYS(0.6)	1170	1.4	7.86	370	920	64.5	47.8	14.1	354	0.0208

### 3.5. The Piezoelectric and Dielectric Properties of PZT-BYS( $x$ ) Ceramics

Figure 6a,b shows the effects of  $\text{Sb}_2\text{O}_3$  contents on  $d_{33}$ ,  $k_p$ ,  $\epsilon_{33}^T$  and grain size. In addition, the electrical properties of PZT-BYS( $x$ ) samples sintered at their optimum temperature have been listed in Table 2. From Table 2, it is clear that doping  $\text{Sb}_2\text{O}_3$  into the PZT-BY increased the  $d_{33}$  and  $k_p$  sharply compared to the undoped specimen. This can be explained by factors like the density, grain size and soft effect of  $\text{Sb}_2\text{O}_3$ . Previously, it was observed that pre-synthesized  $\text{BiYO}_3$  acts as a donor

into the PZT ceramics and improves the piezoelectric and dielectric properties. In the present work, incorporating  $\text{Sb}_2\text{O}_3$  into the PZT ceramic further improved the piezoelectric and dielectric properties because it is possible that the  $\text{Sb}^{3+}$  entered into the A-site and facilitated the domain wall movement. A similar observation was also reported by Dutta et al. where they doped  $\text{Sb}^{3+}$  into the  $\text{Pb}^{2+}$  site [20]. Additionally, The  $\text{Sb}_2\text{O}_3$ -doped specimen shows higher sintered density ( $7.96 \text{ g/cm}^3$  at  $x = 0.1$ ) than the undoped specimen ( $7.91 \text{ g/cm}^3$  at  $x = 0.0$ ). As a result, adding  $\text{Sb}_2\text{O}_3$  into the PZT improved the  $d_{33}$  and  $k_p$  sharply (at  $x = 0.1$ ) compared to the undoped specimen (at  $x = 0.0$ ). A detailed explanation of increasing piezoelectric, dielectric and ferroelectric behavior of the  $\text{Sb}_2\text{O}_3$ -doped sample will be discussed in the next paragraph.

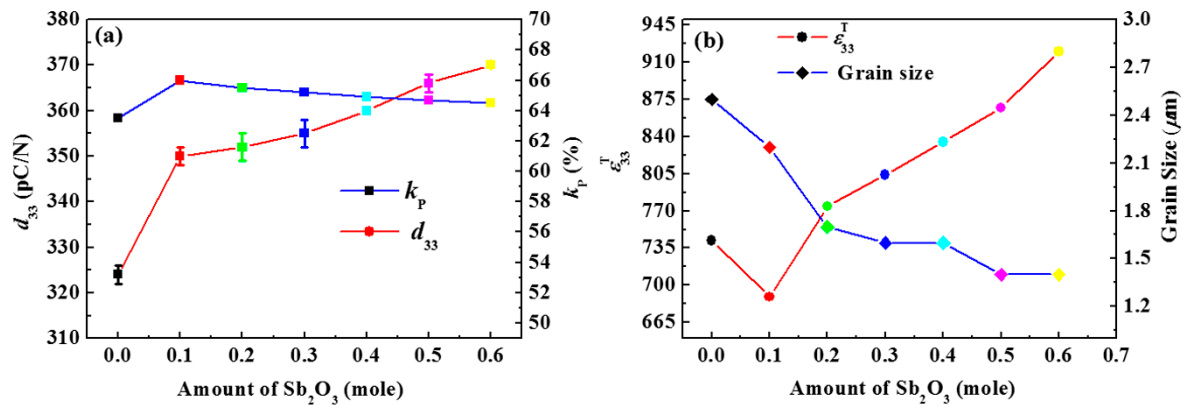


**Figure 6.** Variation of (a)  $d_{33}$  and  $k_p$ ; (b)  $\epsilon_{33}^T$  and grain size as a function of  $\text{Sb}_2\text{O}_3$  contents of PZT-BYS(x) ceramics.

In Figure 6a, it is clear that the  $d_{33}$  and the  $k_p$  increase with increasing amount of  $\text{Sb}_2\text{O}_3$ . The increased density and homogeneous grain size might be a reason for high  $d_{33}$  and  $k_p$ . The increasing behavior of  $d_{33}$  with the addition of  $\text{Sb}_2\text{O}_3$  into PZT was also explained by Zhou et al. [14]. In general, donor doping in PZT is expected to increase the  $d_{33}$  and the  $k_p$  values, which is a soft effect [25]. In the previous work, it was observed that  $\text{BiYO}_3$  acts as a grain growth inhibitor as well as a donor in the vicinity of grains which improve  $d_{33}$  and  $k_p$  in the PZT-BY system [13]. In the present case, similar trends of  $d_{33}$  and  $k_p$  were also observed. Furthermore, the increasing tendency of  $d_{33}$  can be explained by the presence of second phases, as shown in Figure 1a.

It is possible that the second phases of  $\text{Y}_3\text{Sb}_5\text{O}_{12}$ ,  $\text{Bi}_2\text{O}_3$ ,  $\text{Y}_2\text{O}_3$ , and  $\text{BiSbO}_4$ , as shown in Figure 1a, dissociate at the higher sintering temperature. It can be speculated that  $\text{Bi}^{3+}$ ,  $\text{Y}^{3+}$  and  $\text{Sb}^{3+}$  enter into the  $\text{Pb}^{2+}$  site as donor ions in the PZT system to create A-site vacancies in the lattice. Similarly, a donor doping effect of  $\text{Sb}^{3+}$  was reported by Dutta et al. [20]. They studied the structural, dielectric and electrical properties of PZT ceramic extensively to find out the effect of double-doping ( $\text{La}^{3+}$  and  $\text{Sb}^{3+}$ ) at the  $\text{Pb}^{2+}$ -site of PZT. Therefore, in the present work, A-site vacancies reduce the concentration of intrinsic oxygen vacancies during sintering and introduce lead vacancies to maintain the charge neutrality. These cation vacancies would, therefore, increase the mobility of the domain wall [26]. The change in the mobility of the domain wall by cation vacancies improves the  $d_{33}$ , because displacement is sufficient. Therefore,  $d_{33}$  increases with increasing  $\text{Sb}_2\text{O}_3$  content due to the increased concentration of the second phase in the PZT-BYS(x) system.

This increase in  $d_{33}$  by doping was also observed in a typical soft type of PZT system [26,27]. On the contrary, the value of  $k_p$  reached the maximum value of 66.0% at  $x = 0.1$ , whereby it decreased slightly on further addition of  $\text{Sb}_2\text{O}_3$ . The grain size effect could be the predominant factor in this case. Ichinose and Kimura [28] reported that Nb and partially substituted Sb-doped PZT shows the maximum electrical properties at a grain size of 2–3  $\mu\text{m}$ . The deterioration of  $k_p$  with decreasing grain size is probably related to the fewer domains and less mobile domain walls. As a result, a slight decrease in  $k_p$  was observed at higher  $\text{Sb}_2\text{O}_3$  ( $x > 0.1$ ) contents.

Figure 6b shows the variation of  $\epsilon_{33}^T$  and grain size as a function of  $\text{Sb}_2\text{O}_3$  contents. It is clear that  $\epsilon_{33}^T$  varies from those of the piezoelectric properties. The  $\epsilon_{33}^T$  sharply decreases as the grain size decreases from  $\sim 2.5 \mu\text{m}$  (at  $x = 0$ ) to  $2.2 \mu\text{m}$  (at  $x = 0.1$ ), while it increases slightly with a decreasing grain size of  $\sim 1.7 \mu\text{m}$  at  $x = 0.2$ . A further increase in the  $\text{Sb}_2\text{O}_3$  content decreases the grain size to  $\sim 1.4 \mu\text{m}$ , and dielectric constants increased sharply. This type of dielectric anomaly was previously explained by the effect of grain sizes [13,29–34]. Martirenat et al. [29] reported that the dielectric constant of  $\text{BaTiO}_3$  and PZT could be varied at different ranges of grain size. Okazaki and Nagata [34,35] reported that  $\epsilon_{33}^T$  at room temperature increases within a critical range of grain size. Similar behavior was also explained by many earlier investigations of grain size effects [35,36]. They reported that there was a microstructure transition region between  $1.3 \mu\text{m}$  and  $2.7 \mu\text{m}$ . Within this range,  $\epsilon_{33}^T$  decreases with decreasing grain size and increases with increasing grain size [36]. Therefore, in the present work,  $\epsilon_{33}^T$  decreases with the PZT–BYS(0.1) composition because grain size decreases from  $\sim 2.5 \mu\text{m}$  to  $2.2 \mu\text{m}$ . As the grain size decreases below critical values, the structure is changed, and the internal stress would be expected to increase. This in turn suggests that the dielectric constant increases with decreasing grain size for higher  $\text{Sb}_2\text{O}_3$  content.

Further evidence for the  $\text{Sb}_2\text{O}_3$  doping and grain size effects are obtained by examining the polarization-electric field ( $P$ - $E$ ) curve at room temperature and shown in Figure 7a. The values of  $P_r$  and  $E_c$  are determined from the measured  $P$ - $E$  loops. The variation of  $P_r$  and  $E_c$  for undoped and  $\text{Sb}_2\text{O}_3$ -doped PZT–BYS( $x$ ) samples sintered at optimum temperatures are shown in Figure 7b. At 0.1 moles of  $\text{Sb}_2\text{O}_3$  content, a relatively higher  $P_r$  and lower  $E_c$  were observed. The relatively higher  $P_r$  and lower  $E_c$  at  $x = 0.1$  could be explained by high mobility of domain walls achieved by suppression of the oxygen vacancies. Upon further increase of  $\text{Sb}_2\text{O}_3$  content,  $E_c$  and  $P_r$  increases sharply. Above 0.1 moles of  $\text{Sb}_2\text{O}_3$ , the grain size decreases from  $2.2 \mu\text{m}$  to around  $1.7\text{--}1.4 \mu\text{m}$ . As a result, the clamping effect caused by internal stress below a critical grain size increases the  $E_c$ . By contrast, the increasing behavior of  $P_r$  with increasing  $\text{Sb}_2\text{O}_3$  content can be explained by the presence of second phases, which is similar to the behavior of  $d_{33}$ . It is believed that, at the higher sintering temperature, the second phases are dissociated. According to the similarities of ionic radius, the dissociated phase produces cation vacancies in PZT–BYS( $x$ ) as explained for the behavior of  $d_{33}$  as a function of  $\text{Sb}_2\text{O}_3$  content (see Figure 6a). As a result of cation vacancies, the mobility of the domain wall increases [26] due to the sufficient displacement, which finally increases the  $P_r$ . Therefore,  $P_r$  increases at higher  $\text{Sb}_2\text{O}_3$  content due to the higher concentration of the second phase in the PZT–BYS( $x$ ) system. These results are in agreement with a previous analysis of piezoelectric/dielectric properties.

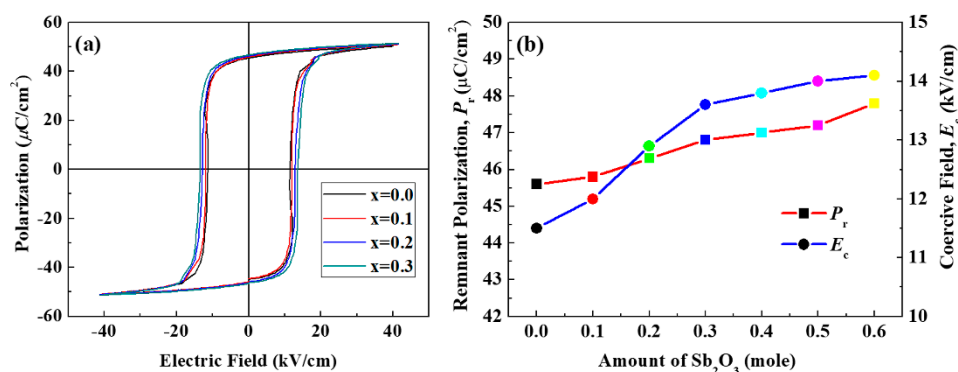


**Figure 7.** (a) Polarization-electric ( $P$ - $E$ ) hysteresis loops, (b)  $P_r$  and  $E_c$  measured from their corresponding hysteresis loops of PZT–BYS( $x$ ) ceramics.

The dielectric constant ( $\epsilon_{33}^T$ ) of PZT–BYS( $x$ ) ceramics as a function of temperature is shown in Figure 8. The  $\epsilon_{33}^T$  was almost constant up to  $300 \text{ }^\circ\text{C}$ , and then increased gradually to a maximum value  $\epsilon_{33}^T(\text{max})$  at Curie temperature ( $T_C$ ). The  $T_C$  of pure PZT is about  $\sim 360 \text{ }^\circ\text{C}$ . It is well known that

cubic phase addition to PZT reduces  $T_C$ , but in our recent work where BY was added into the PZT system,  $T_C$  increased [13]. This anomaly was explained in terms of internal stress, which retarded the ferroelectric and paraelectric transition. In the present case,  $\text{Sb}_2\text{O}_3$ -doping has been shown to produce a linear reduction in  $T_C$ . In Figure 8, it is clear that the  $\epsilon_{33}^T(\text{max})$  sharply decreases as the content of  $\text{Sb}_2\text{O}_3$  increases and the dielectric peaks broaden around  $T_C$ , which is similar to previous observations [13,37]. Similarly, Dutta et al. also explained that the broadening of the dielectric peak and variation of  $\epsilon_{33}^T(\text{max})$  could be attributed to the variation of grain size and some kinds of structural disorder [20]. It has already been established that, with decreasing grain size,  $\epsilon_{33}^T(\text{max})$  decreases, which results in the broadening of the dielectric peak, and shifts in ferroelectrics transition to higher or lower temperature sides [20,29,38].

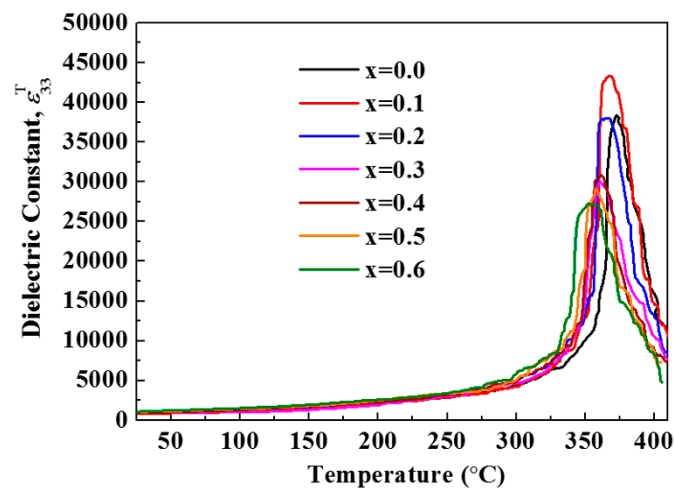


**Figure 8.** Temperature dependence of dielectric constant for different  $\text{Sb}_2\text{O}_3$ -doped PZT-BYS( $x$ ) ceramics.

### 3.6. Feasibility of $\text{Sb}_2\text{O}_3$ -Doped PZT-BYS( $x$ ) Ceramics for Use in an Energy Harvester

The calculated values of  $g_{33}$  and  $d_{33} \times g_{33}$  as a function of  $\text{Sb}_2\text{O}_3$  contents are illustrated in Figure 9. The data of  $g_{33}$  and  $d_{33} \times g_{33}$  for PZT-BYS( $x$ ) has also been shown in Table 3. From Figure 9, it is clear that the addition of  $\text{Sb}_2\text{O}_3$  to the PZT-BYS( $x$ ) system significantly improved  $d_{33} \times g_{33}$ . In general,  $d_{33}$  and  $\epsilon_{33}^T$  increase or decrease simultaneously depending on doping or processing conditions [24]. In the present case, it is observed that increasing behaviors of  $d_{33}$  and  $\epsilon_{33}^T/\epsilon_0$  were not similar at  $x = 0.1$ . For a small amount of  $\text{Sb}_2\text{O}_3$  ( $x = 0.1$ ), a considerable increase in  $d_{33}$  was observed, while  $\epsilon_{33}^T/\epsilon_0$  decreased to its lowest value of 690. Therefore, at  $x = 0.1$  moles of  $\text{Sb}_2\text{O}_3$ , the  $g_{33}$  and  $d_{33} \times g_{33}$  values reached a maximum value of  $57.4 \times 10^{-3} \text{ Vm/N}$  and  $20076 \times 10^{-15} \text{ m}^2/\text{N}$ , respectively. On the other hand, the  $g_{33}$  and  $d_{33} \times g_{33}$  values decreased rapidly at  $x > 0.1$  due to the considerably slower rate of increase in  $d_{33}$  and rapid increase of  $\epsilon_{33}^T/\epsilon_0$ .

**Table 3.** The evaluated values of  $g_{33}$  and  $d_{33} \times g_{33}$  of PZT-BYS( $x$ ) ceramics as a function of  $\text{Sb}_2\text{O}_3$  content at optimum sintered temperature.

Composition	Sintering Temp. (°C)	$g_{33} \times 10^{-3}(\text{Vm/N})$	$d_{33} \times g_{33} (10^{-15} \text{ m}^2/\text{N})$
PZT-BYS(0.0)	1150	49.1	15,824
PZT-BYS(0.1)	1150	57.4	20,075
PZT-BYS(0.2)	1150	51.3	18,044
PZT-BYS(0.3)	1150	49.9	17,686
PZT-BYS(0.4)	1170	48.7	17,513
PZT-BYS(0.5)	1170	47.7	17,431
PZT-BYS(0.6)	1170	45.6	16,908

A list of piezoelectric energy-harvesting parameters reported recently is provided in Table 4 for comparison with the present results. In Table 4, clearly, PZT-BYS( $x$ ) possesses a considerably higher figure of merit with a high  $g_{33}$  value in comparison to the commercially available and recently reported materials. Furthermore, most of the recent works reported a high figure of merit after doping relaxor-type materials into the PZT system. Doping relaxor-type materials into the PZT system evidently causes an abrupt decrease in the  $T_C$ , which limits the application temperature range of these materials [39–43]. On the other hand,  $Sb_2O_3$ -doped PZT-BYS(0.1) shows a high transduction coefficient without much lowering the  $T_C$ . Therefore, it might be concluded that PZT-BYS( $x$ ) with  $x = 0.1$  moles of  $Sb_2O_3$  content could be considered as a good candidate material for piezoelectric energy-harvesting devices.

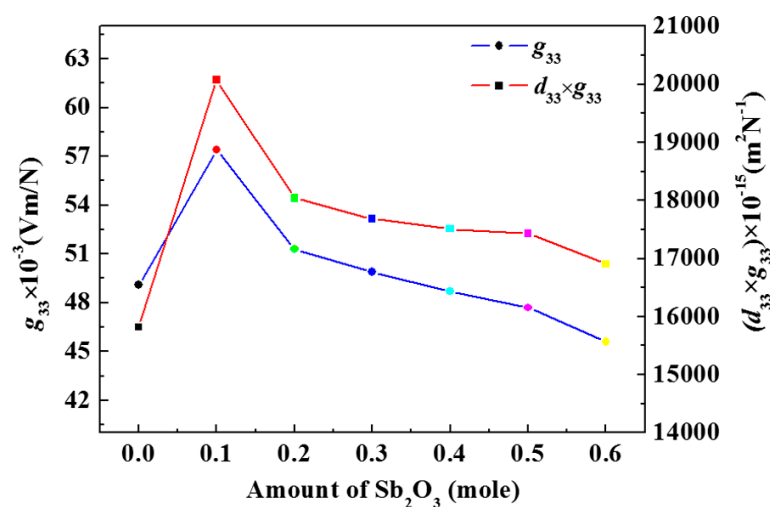


**Figure 9.** Calculated values of  $g_{33}$  and  $d_{33} \times g_{33}$  of PZT-BYS( $x$ ) ceramics as a function of different  $Sb_2O_3$  contents.

**Table 4.** A comparison between the present work and recently reported piezoelectric ceramic materials for energy-harvesting applications.

Composition	$g_{33} \times 10^{-3}$ (Vm/N)	$d_{33} \times g_{33}$ ( $10^{-15} \text{ m}^2/\text{N}$ )	$T_C$ ( $^{\circ}\text{C}$ )	Ref.
0.9Pb(Zr <sub>0.56</sub> Ti <sub>0.44</sub> )O <sub>3</sub> -0.1Pb[(Zn <sub>0.8</sub> Ni <sub>0.2</sub> ) <sub>1/3</sub> Nb <sub>2/3</sub> ]O <sub>3</sub> + 2mol% MnO <sub>2</sub>	83	18,456	~315	41
(0.65 + y)Pb(Zr <sub>0.47</sub> Ti <sub>0.53</sub> )-(0.35 - y)Pb[(Ni <sub>1-x</sub> Zn <sub>x</sub> ) <sub>1/3</sub> Nb <sub>2/3</sub> ]O <sub>3</sub>	36	20,056	...	42
0.72Pb(Zr <sub>0.47</sub> Ti <sub>0.53</sub> )O <sub>3</sub> -0.28Pb[(Zn <sub>0.45</sub> Ni <sub>0.55</sub> ) <sub>1/3</sub> Nb <sub>2/3</sub> ]O <sub>3</sub>	35	13,051	...	43
Pb <sub>0.98</sub> La <sub>0.02</sub> (NiSb) <sub>0.05</sub> [(Zr <sub>0.52</sub> Ti <sub>0.48</sub> ) <sub>0.995</sub> ]O <sub>3</sub>	36.8	16,570	...	16
0.99Pb(Zr <sub>0.53</sub> Ti <sub>0.47</sub> )O <sub>3</sub> -0.01BiYO <sub>3</sub>	53	18,549	373	13
0.99Pb(Zr <sub>0.53</sub> Ti <sub>0.47</sub> )O <sub>3</sub> -0.01Bi(Y <sub>0.9</sub> Sb <sub>0.1</sub> )O <sub>3</sub>	57.4	20,075	369	present

#### 4. Conclusions

The present study has shown that the addition of  $Sb_2O_3$  to 0.99Pb(Zr<sub>0.53</sub>Ti<sub>0.47</sub>)O<sub>3</sub>-0.01Bi(Y<sub>1-x</sub>Sb<sub>x</sub>)O<sub>3</sub> [PZT-BYS( $x$ )] ceramics ( $0 \leq x \leq 0.6$ ) has significantly improved their energy-harvesting properties. The comparative study between doping  $Sb_2O_3$  and  $Sb_2O_5$  into the PZT-BYS( $x$ ) revealed the feasibility of both ceramics for energy harvesting when an appropriate sintering condition is maintained. It was observed that doping  $Sb_2O_3$  into PZT-BYS( $x$ ) while maintaining the oxygen-rich sintering atmosphere had a significant influence on the dielectric and piezoelectric characteristics. All the  $Sb_2O_3$ -doped PZT-BYS( $x$ ) ceramics could be well sintered to high densities at temperatures between 1150 and 1170  $^{\circ}\text{C}$ . The XRD analysis of the sintered sample indicated a pure solid solution of PZT-BYS( $x$ ) without any second phases. The microstructures of the sintered samples were uniform and dense and consistent with the measured density. The Curie temperature of

the ceramics was shown to produce a linear reduction with increasing  $\text{Sb}_2\text{O}_3$  contents, but it is still high enough to use for high-temperature applications. The observed piezoelectric properties were in agreement with the measured  $P$ - $E$  hysteresis loops. A maximum  $d_{33}$  of 370 pC/N at  $x = 0.6$  moles and a maximum  $k_p$  of 66% at  $x = 0.1$  moles were observed. It was also observed that the  $\epsilon_{33}^T$  (690) sharply decreased at  $x = 0.1$  while maintaining relatively higher  $d_{33}$  (350 pC/N), which is a highly demanding piezoelectric characteristic for energy-harvesting. The relatively higher  $d_{33}$  and lower  $\epsilon_{33}^T$  at  $x = 0.1$  resulted in an optimum value of  $g_{33} = 57.4 \times 10^{-3}$  Vm/N and  $d_{33} \times g_{33} = 20075 \times 10^{-15}$  m<sup>2</sup>/N, which is high among recently reported work. Therefore, the newly reported ceramic composition of  $0.99\text{Pb}(\text{Zr}_{0.53}\text{Ti}_{0.47})\text{O}_3-0.01\text{Bi}[\text{Y}_{(1-x)}\text{Sb}_x]\text{O}_3$  could be a promising material for future study to be used in an energy harvester.

**Acknowledgments:** The research was supported by a grant from the Regional Innovation Center (RIC) Program which was conducted by the Ministry of Trade, Industry & Energy of the Korean Government.

**Author Contributions:** Iqbal Mahmud and Man-Soon Yoon designed the experiment. Iqbal Mahmud performed the experiments, analyzed data and wrote the manuscript. Man-Soon Yoon advised regarding data analysis and edited the manuscript. Soon-Chul Ur supervised the research work, advised concerning the study, and edited the manuscript.

**Conflicts of Interest:** The authors declare no conflict of interest.

## References

- Kang, M.G.; Jung, W.S.; Kang, C.Y.; Yoon, S.J. Recent progress on PZT based piezoelectric energy harvesting technologies. *Actuators* **2016**, *5*, 5. [[CrossRef](#)]
- Tang, G.; Yang, B.; Hou, C.; Li, G.; Liu, J.; Chen, X.; Yang, C. A piezoelectric micro generator worked at low frequency and high acceleration based on PZT and phosphor bronze bonding. *Sci. Rep.* **2016**, *6*, 1–10. [[CrossRef](#)] [[PubMed](#)]
- Almusallama, A.; Luob, Z.; Komolafea, A.; Yanga, K.; Robinsonc, A.; Toraha, R.; Beeby, S. Flexible piezoelectric nano-composite films for kinetic energy harvesting from textiles. *Nano Energy* **2017**, *33*, 146–156. [[CrossRef](#)]
- Ramadan, K.S.; Sameoto, D.; Evoy, S. A review of piezoelectric polymers as functional materials for electromechanical transducers. *Smart Mater. Struct.* **2014**, *23*, 1–26. [[CrossRef](#)]
- Li, H.; Tian, C.; Deng, Z.D. Energy harvesting from low frequency applications using piezoelectric materials. *Appl. Phys. Rev.* **2014**, *1*, 1–19. [[CrossRef](#)]
- Lupascu, D.C. *Fatigue in Ferroelectric Ceramics and Related Issues*; Springer: Berlin, Germany, 2004; pp. 43–46.
- Yuan, D.; Yang, Y.; Hu, Q.; Wang, Y. Structures and properties of  $\text{Pb}(\text{Zr}_{0.5}\text{Ti}_{0.5})\text{O}_3$ - $\text{Pb}(\text{Zn}_{1/3}\text{Nb}_{2/3})\text{O}_3$ - $\text{Pb}(\text{Ni}_{1/3}\text{Nb}_{2/3})\text{O}_3$  ceramics for energy harvesting devices. *J. Am. Ceram. Soc.* **2014**, *97*, 3999–4004. [[CrossRef](#)]
- Yoon, S.J.; Kang, H.W.; Kucheiko, S.I.; Kim, H.J.; Jung, H.J.; Lee, D.K.; Ahn, H.K. Piezoelectric properties of  $\text{Pb}[\text{Zr}_{0.45}\text{Ti}_{0.5-x}\text{Lu}_x(\text{Mn}_{1/3}\text{Sb}_{2/3})_{0.05}]\text{O}_3$  ceramics. *J. Am. Ceram. Soc.* **1998**, *81*, 2473–2476. [[CrossRef](#)]
- Choi, C.H.; Seo, I.T.; Song, D.; Jang, M.S.; Kim, B.Y.; Nahm, S.; Sung, T.H.; Song, H.C. Relation between piezoelectric properties of ceramics and output power density of energy harvester. *J. Eur. Ceram. Soc.* **2013**, *33*, 1343–1347. [[CrossRef](#)]
- Lonkar, C.M.; Premkumar, S.; Kharat, D.K.; Kumar, H.H.; Prasad, S.; Balasubramanian, K. Effect of La on piezoelectric properties of  $\text{Pb}(\text{Ni}_{1/3}\text{Sb}_{2/3})\text{O}_3$ - $\text{Pb}(\text{ZrTi})\text{O}_3$  ferroelectric ceramics. *J. Mater. Sci. Mater. Electron.* **2013**, *24*, 1989–1993. [[CrossRef](#)]
- Xu, R.; Kim, S.G. Figures of merits of piezoelectric materials in energy harvesters. In Proceedings of the PowerMEMS, Atlanta, GA, USA, 2–5 December 2012.
- Priya, S. Criterion for material selection in design of bulk piezoelectric energy harvesters. *IEEE Trans. Ultrason. Ferroelectr. Freq. Control* **2010**, *57*, 2610–2612. [[CrossRef](#)] [[PubMed](#)]
- Yoon, M.S.; Mahmud, I.; Ur, S.C. Phase formation, microstructure and piezoelectric/dielectric properties of  $\text{BiYO}_3$  doped  $\text{Pb}(\text{Zr}_{0.53}\text{Ti}_{0.47})\text{O}_3$  for piezoelectric energy harvesting devices. *Ceram. Int.* **2013**, *39*, 8581–8588. [[CrossRef](#)]
- Zhou, T.; Wang, S.; Gu, H.; He, Y.; Kuang, A.; Sun, W. The effect of doping  $\text{Sb}_2\text{O}_3$  in high  $d_{33} \bullet g_{33}$  PZT piezoelectric ceramics. *Ferroelectrics* **1997**, *195*, 101–104. [[CrossRef](#)]

15. Rai, R.; Sharma, S. Structural and dielectric properties of Sb-doped PLZT ceramics. *Ceram. Int.* **2004**, *30*, 1295–1299. [[CrossRef](#)]
16. Lonkar, C.M.; Kharat, D.K.; Kumar, H.H.; Prasad, S.; Balasubramanian, K. Effect of sintering time on dielectric and piezoelectric properties of Lanthanum doped  $\text{Pb}(\text{Ni}_{1/3}\text{Sb}_{2/3})\text{-PbZrTiO}_3$  ferroelectric ceramics. *Def. Sci. J.* **2013**, *63*, 418–422. [[CrossRef](#)]
17. Zahi, S.; Bouaziz, R.; Abdessalem, N.; Boutarfaia, A. Dielectric and piezoelectric properties of  $\text{PbZrO}_3\text{-PbTiO}_3\text{-Pb}(\text{Ni}_{1/3}\text{Sb}_{2/3})\text{O}_3$  ferroelectric ceramic system. *Ceram. Int.* **2003**, *29*, 35–39. [[CrossRef](#)]
18. Luan, N.D.T.; Vuong, L.D.; Chanh, B.C. Microstructure, ferroelectric and piezoelectric properties of PZT-PMnSbN ceramics. *Int. J. Mater. Chem.* **2013**, *3*, 51–58.
19. Choia, W.Y.; Ahn, J.H.; Lee, W.J.; Kim, H.G. Electrical properties of Sb-doped PZT films deposited by d.c. reactive sputtering using multi-targets. *Mater. Lett.* **1998**, *37*, 119–127. [[CrossRef](#)]
20. Dutta, S.; Choudhary, R.N.P.; Sinha, P.K. Electrical properties of antimony doped PLZT ceramics prepared by mixed-oxide route. *J. Alloys Compd.* **2006**, *426*, 345–351. [[CrossRef](#)]
21. Dutta, S.; Choudhary, R.N.P.; Sinha, P.K. Studies on structural, electrical and electromechanical properties of  $\text{Sb}^{3+}$ -modified PLZT. *Mater. Sci. Eng. B* **2004**, *113*, 215–223. [[CrossRef](#)]
22. Yoon, S.J.; Choi, J.W.; Choi, J.Y.; Dandan, W.; Li, Q.; Yang, Y. Influences of donor dopants on the properties of PZT-PMS-PZN piezoelectric ceramics sintered at low temperatures. *J. Korean Phys. Soc.* **2010**, *57*, 863–867.
23. Shannon, R.D. Revised effective ionic radii and systematic studies of interatomic distances in halides and chalcogenides. *Acta Cryst.* **1976**, *A32*, 751–767. [[CrossRef](#)]
24. Uchino, K.; Takasu, T. Property variation of piezoelectric ceramics with microstructure. *Inspec* **1986**, *10*, 29–33.
25. Slouka, C.; Kainz, T.; Navickas, E.; Walch, G.; Hutter, H.; Reichmann, K.; Fleig, J. The effect of acceptor and donor doping on oxygen vacancy concentrations in lead zirconate titanate (PZT). *Materials* **2016**, *9*, 945. [[CrossRef](#)] [[PubMed](#)]
26. Tani, T.; Watanabe, N.; Takatori, K.; Hori, S. Piezoelectric and dielectric properties for doped lead zirconate titanate ceramics under strong electric field. *J. Appl. Phys.* **1994**, *33*, 5352–5355. [[CrossRef](#)]
27. Takahashi, S.; Hirose, S.; Uchino, K. Stability of PZT piezoelectric ceramics under vibration level change. *J. Am. Ceram. Soc.* **1994**, *77*, 2429–2432. [[CrossRef](#)]
28. Ichinose, N.; Kimura, M. Preparation and properties of lead zirconate-titanate piezoelectric ceramics using ultrafine particles. *Jpn. J. Appl. Phys.* **1991**, *30*, 2220–2223. [[CrossRef](#)]
29. Martirenat, H.T.; Burfoot, J.C. Grain-size effects on properties of some ferroelectric ceramics. *J. Phys. C Solid State Phys.* **1974**, *7*, 3182–3192. [[CrossRef](#)]
30. Shirane, G.; Sawaguchi, E.; Takagi, Y. Dielectric properties of lead zirconate. *J. Phys. Soc. Jpn.* **1951**, *6*, 208–209. [[CrossRef](#)]
31. Okazaki, K.; Nagata, K. Mechanical behaviour of materials. *J. Soc. Mater. Sci. Jpn.* **1972**, *4*, 404.
32. Okazaki, K.; Nagata, K. Effects of grain size and porosity on electrical and optical properties of PLZT ceramics. *J. Am. Ceram. Soc.* **1973**, *56*, 82–86. [[CrossRef](#)]
33. Lee, K.G.S.; ShROUT, T.R.; Venkataramani, S. Fabrication of fine-grain piezoelectric ceramics using reactive calcination. *J. Mater. Sci.* **1991**, *26*, 4411–4415.
34. Ai, Z.; Hou, Y.; Zheng, M.; Zhu, M. Effect of grain size on the phase structure and electrical properties of PZT-PNZN quaternary systems. *J. Alloys Compd.* **2014**, *617*, 222–227. [[CrossRef](#)]
35. Arlt, G. The influence of microstructure on the properties of ferroelectric ceramics. *Ferroelectrics* **1990**, *104*, 217–227. [[CrossRef](#)]
36. Kang, B.S.; Choi, D.G.; Choi, S.K. Effects of grain size on pyroelectric and dielectric properties of  $\text{Pb}_{0.9}\text{La}_{0.1}\text{TiO}_3$  ceramic. *J. Korean Phys. Soc.* **1998**, *32*, S232–S234.
37. Chamola, A.; Singh, H.; Naithani, U.C. Study of  $\text{Pb}(\text{Zr}_{0.65}\text{Ti}_{0.35})\text{O}_3$  (PZT(65/35)) doping on structural, dielectric and conductivity properties of  $\text{BaTiO}_3$  (BT) ceramics. *Adv. Mater. Lett.* **2011**, *2*, 148–152. [[CrossRef](#)]
38. Miga, S.; Wojcik, K. Investigation of the diffuse phase transition in PLZT X/65/35 ceramics,  $x = 7\text{--}10$ . *Ferroelectrics* **1989**, *100*, 167–173. [[CrossRef](#)]
39. Mahmud, I.; Ur, S.C.; Yoon, M.S. Effects of  $\text{Fe}_2\text{O}_3$  addition on the piezoelectric and the dielectric properties of  $0.99\text{Pb}(\text{Zr}_{0.53}\text{Ti}_{0.47})\text{O}_3\text{-}0.01\text{Bi}(\text{Y}_{1-x}\text{Fe}_x)\text{O}_3$  ceramics for energy-harvesting devices. *J. Korean Phys. Soc.* **2014**, *65*, 133–144. [[CrossRef](#)]

40. Wagner, S.; Kahraman, D.; Kungl, H.; Hoffmann, M.J.; Schuh, C.; Lubitz, K.; Biesenecker, H.M.; Schmid, J.A. Effect of temperature on grain size, phase composition, and electrical properties in the relaxor-ferroelectric-system  $\text{Pb}(\text{Ni}_{1/3}\text{Nb}_{2/3})\text{O}_3\text{-Pb}(\text{Zr,Ti})\text{O}_3$ . *J. Appl. Phys.* **2005**, *98*, 024102. [[CrossRef](#)]
41. Islam, R.A.; Priya, S. High energy density composition in the system PZT-PZNN. *J. Am. Ceram. Soc.* **2006**, *89*, 3147–3156. [[CrossRef](#)]
42. Seo, I.T.; Cha, Y.J.; Kang, I.Y.; Choi, J.H.; Nahm, S.; Seung, T.H.; Paik, J.H. High energy density piezoelectric ceramics for energy harvesting devices. *J. Am. Ceram. Soc.* **2011**, *94*, 3629–3631. [[CrossRef](#)]
43. Jeong, Y.H.; Kim, K.B.; Lee, Y.J.; Choi, J.H.; Kim, B.I.; Paik, J.H.; Nahm, S. Ferroelectric and Piezoelectric Properties of  $0.72\text{Pb}(\text{Zr}_{0.47}\text{Ti}_{0.53})\text{O}_3\text{-}0.28\text{Pb}[(\text{Zn}_{0.45}\text{Ni}_{0.55})_{1/3}\text{Nb}_{2/3}]\text{O}_3$ . *Jpn. J. Appl. Phys.* **2012**, *51*, 9S2. [[CrossRef](#)]



© 2017 by the authors. Licensee MDPI, Basel, Switzerland. This article is an open access article distributed under the terms and conditions of the Creative Commons Attribution (CC BY) license (<http://creativecommons.org/licenses/by/4.0/>).